Applied Surface Science 301 (2014) 475–480

Contents lists available at ScienceDirect

Applied Surface Science

journal homepage: www.elsevier.com/locate/apsusc

Structure and properties of uranium oxide thin films deposited by pulsed dc magnetron sputtering

Jianliang Lin[a,*], Isaac Dahan[b], Billy Valderrama[c], Michele V. Manuel[c]

[a] Materials Engineering Dept, Southwest Research Institute, San Antonio, TX 78238, USA
[b] Nuclear Research Center, Beer-Sheva 84190, Israel
[c] Department of Materials Science and Engineering, University of Florida, Gainesville, FL 32611, USA

ARTICLE INFO

Article history:
Received 20 November 2013
Received in revised form 19 February 2014
Accepted 19 February 2014
Available online 28 February 2014

Keywords:
Uranium oxide
Thin films
Pulsed dc magnetron sputtering
Hardness
Annealing

ABSTRACT

Crystalline uranium oxide thin films were deposited in an unbalanced magnetron sputtering system by sputtering from a depleted uranium target in an $Ar+O_2$ mixture using middle frequency pulsed dc magnetron sputtering. The substrate temperature was constantly maintained at 500 °C. Different uranium oxide phases (including UO_{2-x}, UO_2, U_3O_7 and U_3O_8) were obtained by controlling the percentage of the O_2 flow rate to the total gas flow rate (f_{O_2}) in the chamber. The crystal structure of the films was characterized using X-ray diffraction and the microstructure of the films was studied using transmission electron microscopy and atom probe tomography. When the f_{O_2} was below 10%, the film contains a mixture of metallic uranium and UO_{2-x} phases. As the f_{O_2} was controlled in the range of 10–13%, UO_2 films with a (2 2 0) preferential orientation were obtained. The oxide phase rapidly changed to a mixture of U_3O_7 and U_3O_8 as the f_{O_2} was increased to the range of 15–18%. Further increasing the f_{O_2} to 20% and above, polycrystalline U_3O_8 thin films with a (0 0 1) preferential orientation were formed. The hardness and Young's modulus of the uranium oxide films were evaluated using nanoindentation. The film containing a single UO_2 phase exhibited the maximum hardness of 14.3 GPa and a Young's modulus of 195 GPa. The UO_2 thin film also exhibited good thermal stability in that no phase change was observed after annealing at 600 °C in vacuum for 104 h.

Published by Elsevier B.V.

1. Introduction

Uranium is the heaviest radioactive element which forms a wide range of oxide phases, e.g. UO_2, U_4O_9, U_2O_5, U_3O_8, UO_3, etc. [1]. Among these chemical oxide phases, UO_2 is the most studied oxide form and is mainly used for nuclear reactor fuel [2]. Uranium oxides in the thin film form are of technical importance because they are excellent candidates for studying radioactive damage, and reaction and corrosion products in nuclear fuel [3,4]. Further, uranium oxide thin films exhibit interesting properties, e.g. high melting temperatures, high catalytic activity for the oxidation of carbon monoxide, high reflectivity in the extreme ultraviolet region, and high dielectric constant. These properties make them attractive candidates for catalytic, optical, and semiconductor applications [5–8]. However, the studies for uranium oxide thin films fabrication and characterization are limited due to material handling and storage safety concerns.

Fabrication of thin films with well characterized and controlled uranium oxide phases is important for achieving a better understanding of microstructure, stability and properties of uranium oxide in the thin film form. Vacuum evaporation [9–12], sol–gel [7], solution [3], polmyer-assited deposition [13] and magnetron sputtering [14–16] techniques have been used for depositing uranium oxide thin films since the 1960s. With the magnetron sputtering approach, uranium oxide films can be deposited by directly sputtering from a pure reactor grade sintered UO_2 pellet [14] or by reactive sputtering of a depleted uranium target in an Ar/O_2 atmosphere [15,16]. The typical power sources for magnetron sputtering include continuous direct current magnetron sputtering (DCMS), radio frequency magnetron sputtering (RFMS), and middle frequency pulsed dc magnetron sputtering (PDCMS). Among these sputtering techniques, the PDCMS technique has shown several great advantages. PDCMS provides a stable and arc-free deposition process for oxide film depositions. In addition, the PDCMS plasma contains an increased ion flux with a wide range of ion energy distribution (up to hundreds of eV) as compared to the low plasma density in DCMS [17,18]. These high energetic ions can be usefully utilized to improve the adhesion and density of the films [17].

* Corresponding author. Tel.: +1 210 522 5183; fax: +1 210 522 6220.
E-mail addresses: jlin@swri.org, jianliang.lin@swri.org (J. Lin).

http://dx.doi.org/10.1016/j.apsusc.2014.02.106
0169-4332/Published by Elsevier B.V.

However, studies on the deposition of uranium oxide thin films with controlled oxide phases using PDCMS is limited.

In this paper, we report the approach to deposit uranium oxide thin films with different oxide phases using PDCMS. The crystal phase, microstructure, mechanical properties, and thermal stability of uranium oxide thin films were studied using X-ray diffraction (XRD), field emission scanning electron microscopy (FESEM), transmission electron microscopy (TEM), atom probe tomography (APT), and nanoindentation.

2. Experimental details

The uranium oxide thin films were reactively deposited in an unbalanced magnetron sputtering system by sputtering a depleted uranium target (127 mm in diameter) in an $Ar + O_2$ mixture. The substrates were silicon (Si) (1 0 0) and yttria-stabilized zirconia (YSZ) (1 1 0) single crystal wafers, which were mounted on a substrate holder. The substrate temperature was maintained constantly at 500 °C using a resistor as the heating element. The distance from the substrates to the target was 50 mm. A base pressure less than 1×10^{-4} Pa was achieved before all depositions.

Prior to the film depositions, the substrates were sputter etched in pure Ar plasma at a pressure of 1.3 Pa for 30 min using a pulsed dc voltage of −500 V (100 kHz and 90% duty cycle). For the uranium oxide film depositions, the U target was powered by a pulsed dc power supply (Pinnacle Plus, Advanced Energy, Inc.) at an average target power density of 7 W cm^{-2}. The target voltage waveform is in an asymmetric bipolar shape with a pulsing frequency of 100 kHz and a duty cycle of 90%. During the positive pulse period, the target voltage was reversed to 10% of the nominal negative sputtering voltage. For all depositions, the working pressure was 0.67 Pa. The percentage of the O_2 flow rate to the total gas flow rate (f_{O_2}) was varied from 0 to 30% with a total gas flow rate of 20 sccm. A floating substrate bias voltage was used. The thickness of the obtained uranium oxide films was in the range of 0.7–1.5 μm by adjusting the deposition time from 30 to 60 min for different f_{O_2} percentages.

The crystal structure of the films was characterized using XRD in a Siemens diffractmetor using K_α Cu radiation (35 kV and 25 mA) in conventional Bragg-Brentano mode. The cross-sectional microstructure of the films was characterized by FESEM (JSM-7000F) and TEM (Phillips CM200) using an accelerating voltage of 5 and 200 kV, respectively. Nanoscale chemical composition and microstructure of the UO_2 film deposited at $f_{O_2} = 10\%$ were analyzed using APT. Samples for APT were prepared by focused ion beam milling (FEI 3D Quanta) [19]. APT was performed using a CAMECA LEAP 4000× HR instrument operated in pulsed UV laser mode. The experimental conditions used in the atom probe analyses were 50 K temperature, 50 pJ pulse energy, and 100 kHz pulse rate.

The mean hardness and Young's modulus values of the films were measured using a nanoindenter (NanoIndenter XPTM, MTS Systems Corporation) equipped with a diamond Berkovich tip by taking at least 12 effective measurements. The indentation depth was kept constantly below 10% of the film thickness to minimize the substrate effect.

The thermal stability of the UO_2 film deposited at $f_{O_2} = 10\%$ was investigated in situ using heat stage X-ray diffraction (HSXRD) in vacuum. To minimize the oxidation effects, the UO_2 thin film sample was surrounded by titanium (Ti) metal sponge. The testing chamber was vacuumed down to 3×10^{-3} Torr. Then the sample was heated up to 600 °C in 5 min and held at 600 °C for 104 h. The crystal phase of the film was examined in situ using HSXRD.

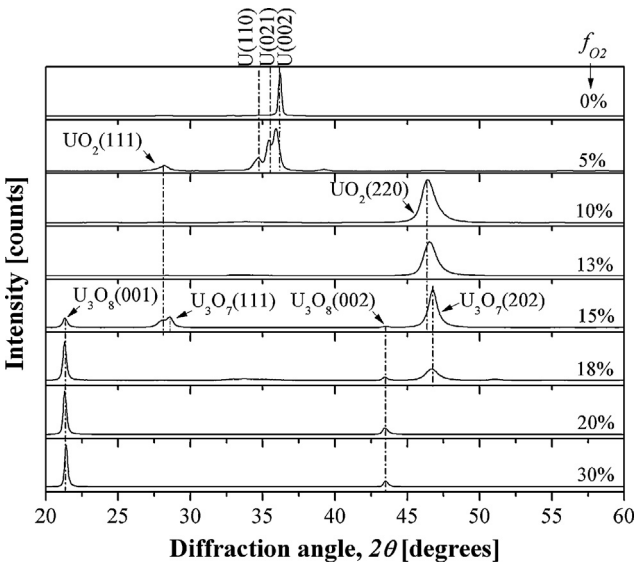

Fig. 1. XRD patterns of uranium oxide films deposited at different f_{O_2} percentages.

3. Results and discussion

3.1. Crystal phase of the uranium oxide films

The XRD patterns of the films deposited at different f_{O_2} percentages are presented in Fig. 1. The metal uranium film deposited in pure Ar ($f_{O_2} = 0$) exhibits α-U structure with a strong (0 0 2) preferential orientation (JCPDF 11-0628). The film deposited at $f_{O_2} = 5\%$ shows a mixture of α-U and cubic UO_2 phases. The dominated α-U phase has three peaks corresponding to the (1 1 0), (0 2 1) and (0 0 2) planes. These diffraction peaks shifted to smaller angles as compared to their standard positions. This fact indicates the distortion of the U lattice due to the incorporation of O atoms in the interstitial sites. In addition, a broad and low intensity peak can also be observed at 28.2° in the diffraction pattern, which corresponds to the (1 1 1) orientation of the cubic UO_2 phase (JCPDF 41-1422).

As f_{O_2} was increased to 10% and 13%, UO_2 films with a (2 2 0) preferential orientation were obtained, as shown in Fig. 1. Many factors affect the texture of thin films, such as the substrate and its temperature during film growth, negative bias voltage, film thickness, and the ion flux and ion energy, etc. For cubic film depositions, the (2 0 0) surfaces are generally expected to grow preferentially because of their low surface energy. However, when additional kinetic or thermal energy is incorporated into the deposition process, higher strain energy in the film will result in orientation changes in the films [17,20]. In this study, the enhanced ion bombardment from the pulsed dc plasma at an elevated temperature (500 °C) likely attributed to the growth of (2 2 0) orientation in the UO_2 films. As compared to the standard (2 2 0) position at 46.97° (JCPDF 41-1422), the (2 2 0) peak of the two UO_2 films slightly shifted to smaller angles. The XRD peak shifting of the films is generally related to the changes of the residual stress and/or the stoichiometry of the films. For the film deposited at $f_{O_2} = 10\%$, the (2 2 0) peak position is at 46.5°, which corresponds to an inter planar spacing of 1.95 Å. For the UO_2 film obtained at a higher f_{O_2} (13%), the (2 2 0) peak slightly shifted to a higher diffraction angle of 46.7°, which corresponds to an inter planar spacing of 1.94 Å. The variation in the inter planar spacing of the UO_2 film deposited at different f_{O_2} indicates that off-stoichiometry UO_2 films can be deposited using reactive pulsed dc magnetron sputtering by carefully controlling the f_{O_2}.

Further increasing the f_{O_2} to 15%, the uranium oxide film showed the formation of mixed oxide phases. The film mainly contains the

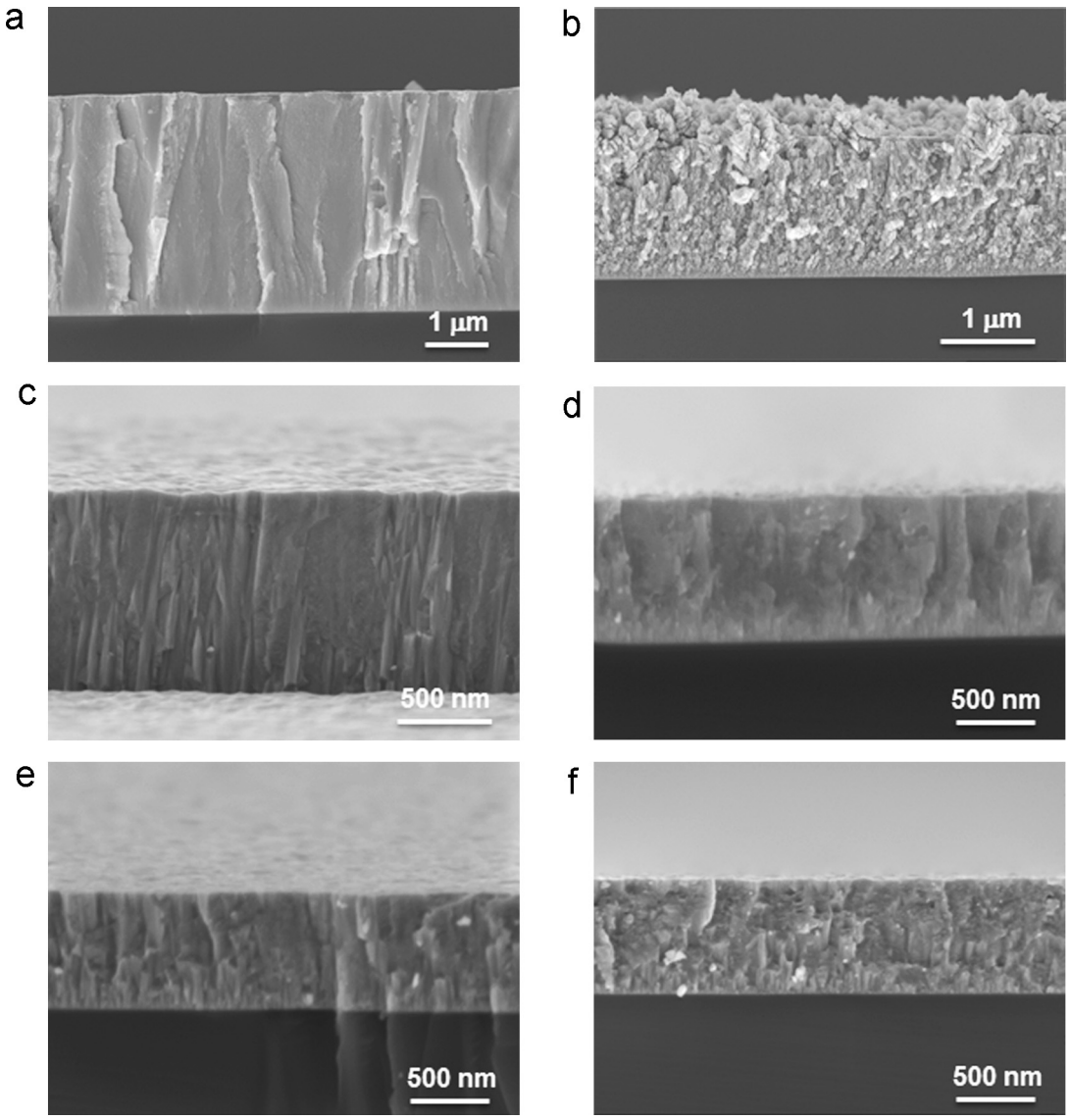

Fig. 2. Cross-sectional SEM micrographs of uranium oxide films deposited at different f_{O_2} percentages: (a) 0%, (b) 5%, (c) 10%, (d) 13%, (e) 15%, and (f) 20%.

tetragonal U_3O_7 phase with (1 1 1) and (2 0 2) reflections (JCPDF 42-1215). In addition, a small amount of UO_2 and U_3O_8 phases can also be identified in this film. When the f_{O_2} was further increased to 18%, the uranium oxide film contains a dominant U_3O_8 phase with (0 0 1) and (0 0 2) diffraction peaks at 21.4° and 43.6°, and a small fraction of the U_3O_7 phase. Further increasing the f_{O_2} to 20 and 30%, the films exhibited a single U_3O_8 phase with preferred (0 0 1) and (0 0 2) parallel planes. However, it is difficult to determine the exact crystal phase of the U_3O_8 film because the (0 0 1) and (0 0 2) peaks of the hexagonal and orthorhombic U_3O_8 phases overlap and thus are convoluted. It also can be seen that the peak width of the U_3O_8 diffraction peaks is narrower than those of the UO_2 films. This is likely related to an increase in the grain size of the U_3O_8 films, as will be discussed later.

3.2. Microstructure of the uranium oxide films

Fig. 2 presents the cross-sectional SEM micrographs of the uranium oxide thin films deposited at different f_{O_2} percentages at 500 °C. Fig. 3 shows the deposition rate of the uranium oxide thin films as a function of f_{O_2} as calculated from the thickness of the film and the deposition time. The pure α-U film exhibited dense microstructure with large crystals (Fig. 2a) and the highest deposition rate of 62 nm/min (Fig. 3). The deposition rate for the film deposited at f_{O_2} = 5% dropped down to 44 nm/min. The film exhibited two distinguishable grain morphologies, including the short

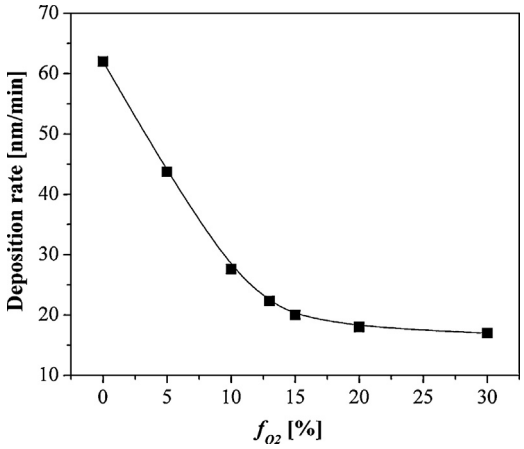

Fig. 3. Deposition rate of uranium oxide films as a function of f_{O_2}.

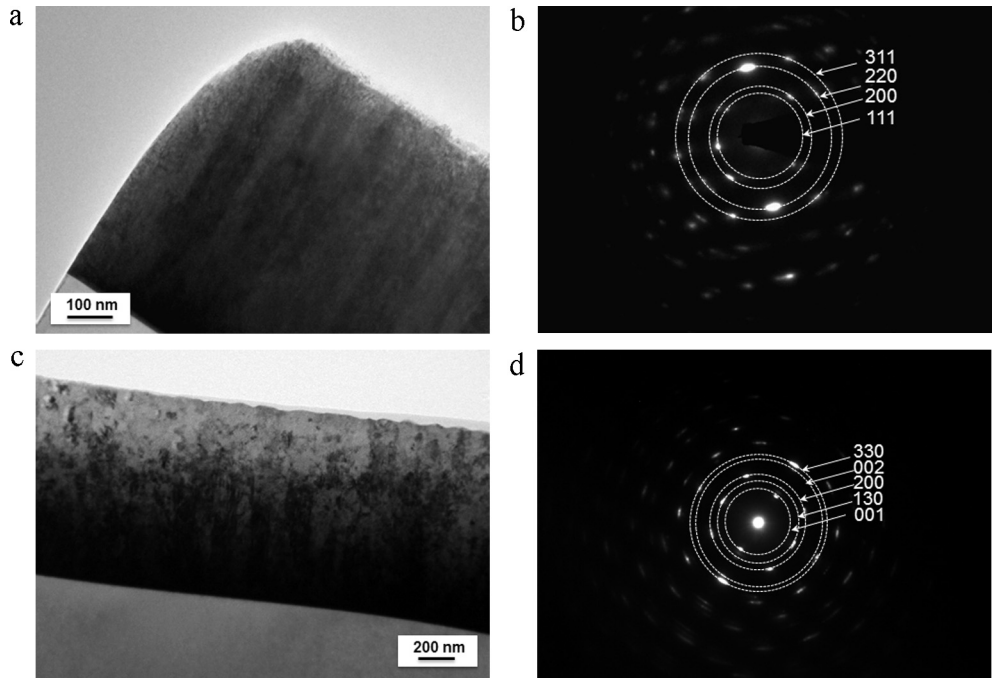

Fig. 4. Cross-sectional TEM micrographs and the SAED patterns of UO_2 film (a and b) and U_3O_8 film (c and d) deposited at f_{O_2} = 10% and 20%, respectively.

columnar grains and the porous equiaxed grains (Fig. 2b). The formation of this type of microstructure is probably related to the co-existence of metallic α-U and UO_2 phases in the film, as confirmed from the XRD pattern (Fig. 1).

As shown in Fig. 2c, the UO_2 film deposited at f_{O_2} = 10% exhibited dense columnar grain structure with the width of the columnar grains in the range of 100–200 nm. The film deposited at f_{O_2} = 13% is also a UO_2 film that exhibited very dense structure. The deposition rate for the UO_2 films dropped rapidly to 27.6 nm/min and 22 nm/min as the f_{O_2} was increased to 10 and 13%, respectively. The large drop in the deposition rate is mainly due to the target poisoning effect commonly observed in reactive magnetron sputtering [21].

When the f_{O_2} was increased to 15% and above, the deposition rate of the films remained at the low levels of 17–18 nm/min, as the deposition process was in the poison mode (Fig. 3). The two films deposited at a f_{O_2} of 15 and 20%, which mainly contain the U_3O_7 and U_3O_8 phases, respectively, also exhibited dense microstructure with large equiaxed grains, as shown in Fig. 2e and f, respectively.

Fig. 4 shows the cross-sectional TEM bright-field micrographs and the selected area electron diffraction (SAED) patterns of the UO_2 and U_3O_8 thin films deposited at f_{O_2} = 10% and 20%, respectively. As shown in Fig. 4a, the UO_2 film deposited at f_{O_2} = 10% exhibited dense structure with long columnar grains grown perpendicular to the substrate. The SAED pattern of the film shows discontinued diffraction rings, corresponding to an fcc-type structure associated with (1 1 1), (2 0 0), (2 2 0) and (3 1 1) Bragg reflections for cubic UO_2 (Fig. 4b). There are two elongated diffraction spots for the (2 2 0) reflection, indicating that the film has a preferential (2 2 0) orientation.

For the U_3O_8 film deposited at f_{O_2} = 20%, the film exhibited dense equiaxed grain growth structure (Fig. 4c). The large contrast of the grains indicates the grains contain different orientations. The SAED pattern of the film can be indexed to an hcp-type structure, associated with (0 0 1), (1 3 0), (2 0 0), (0 0 2) and (3 3 0) Bragg reflections for hexagonal U_3O_8 phase.

Both XRD and TEM studies confirmed the successful preparation of UO_2 and U_3O_8 thin films using pulsed dc magnetron sputtering at 500 °C. The microstructure of the UO_2 film deposited at f_{O_2} = 10% was further investigated using High resolution TEM (HRTEM) and APT. Fig. 5 shows a HRTEM image taken from a large columnar grain in the UO_2 film, in which one-dimensional lattice fringes have been observed. The spacing between the lattice fringes was measured to be 1.95 Å, which is close to the standard $d_{(2\,2\,0)}$ (1.93 Å) of the cubic UO_2 crystal. This result indicates that the majority of the UO_2 crystals have the orientation with their (2 2 0) face parallel to the substrate/film interface. This result agrees well with the observations from the XRD (Fig. 1) and SAED pattern (Fig. 4b).

Nanoscale chemical composition and microstructure of the UO_2 film deposited on the YSZ substrate at f_{O_2} = 10% was analyzed using APT. Fig. 6a provides a 1D concentration profile of the UO_2 film at the interface with the YSZ substrate, taken from a cylindrical region of interest of the APT reconstruction presented in Fig. 6b. Fig. 6b

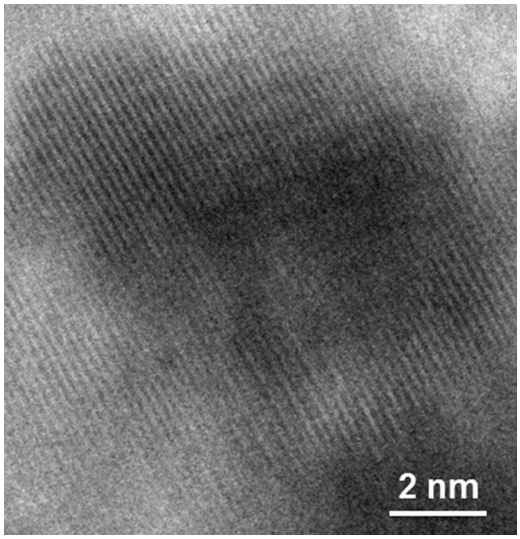

Fig. 5. HRTEM micrograph of the UO_2 film deposited at f_{O_2} = 10%.

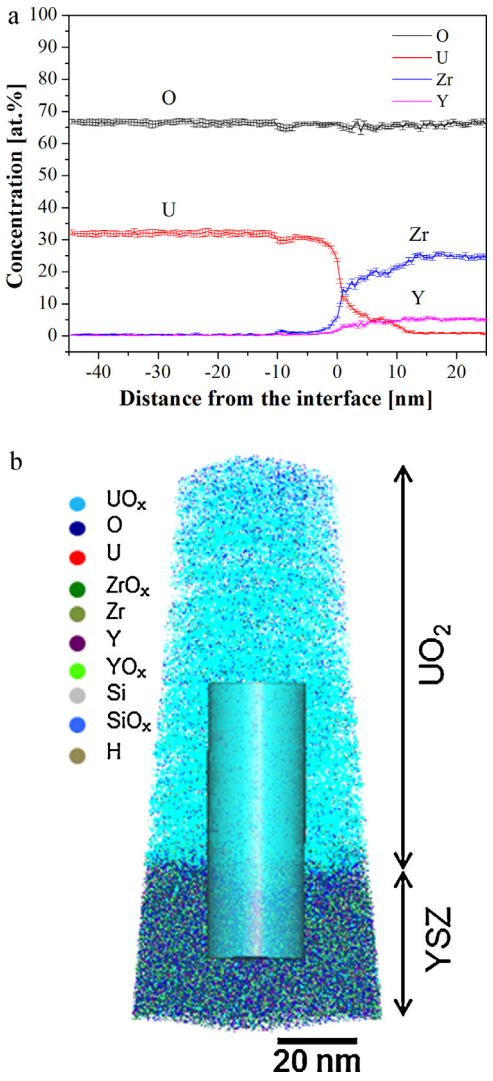

Fig. 6. (a) Atom probe 1-D concentration profile taken from the cylinder shown in the (b) 3D APT reconstruction of the elements in the UO_2/YSZ thin film. Complex ions represented as UO_x, ZrO_x, YO_x, SiO_x where $x = 1$, 2, or 3.

shows the 3D APT reconstruction of the film and substrate and listing the ionic species that were detected, including the following complex ions: UO_x, O, U, ZrO_x, Zr, Y, YO_x, Si SiO_x, where $x = 1$, 2, or 3. The error bars in Fig. 6a were calculated by the standard error, sqrt($p(1-p)/n$), where p is the concentration and n is the sample size. The O content showed a very small variation in the range of 66 to 68 at.%, while the U content is in the range of 32–34 at%. The interface between the UO_2 film and the YSZ substrate exhibited a graded chemical concentration for U. The gradient zone is about 15 nm. The 3D APT reconstruction of the elements in the UO_2 film and YSZ substrate showed a uniform distribution of UO_2. By collecting 6 million ions, the O:U concentration ratio in this region was found to be 2.03.

3.3. Mechanical properties of the uranium oxide films

Fig. 7 shows the hardness and Young's modulus values measured for the uranium oxide films deposited at different f_{O_2} percentages. The hardness and Young's modulus of the metal α-U film are 3 GPa and 84 GPa, respectively. Both values increased to 4.2 GPa and 110 GPa for the UO_x ($x < 2$) film deposited at $f_{O_2} = 5\%$. It is deduced that the solid solution strengthening effect contributed to the increase in the hardness of the UO_x ($x < 2$) film [22].

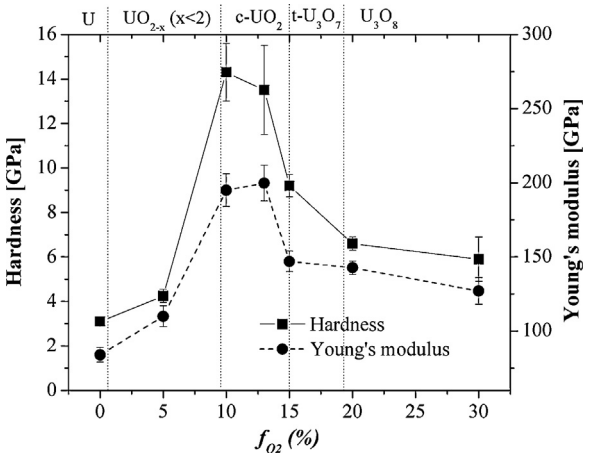

Fig. 7. Hardness and Young's modulus of uranium oxide films deposited at different f_{O_2} percentages.

The hardness and modulus of the film dramatically increased to maximum values of 14.3 GPa and 195 GPa, respectively, for the cubic UO_2 film ($f_{O_2} = 10\%$). As the f_{O_2} was further increased, the hardness and Young's modulus of the uranium oxide films dropped rapidly. For the U_3O_7 and U_3O_8 thin films deposited at $f_{O_2} > 15\%$ the hardness and Young's modulus of the films are in the range of 6–9 GPa and 127–147 GPa, respectively. The nanoindentation study demonstrated that the single phase UO_2 thin film exhibited the highest hardness and Young's modulus among the uranium oxide films with different oxide phases. Also, the hardness of the UO_2 thin films deposited using PDCMS in this study is higher than the values measured on a bulk polycrystalline UO_2 disk (8.3–8.6 GPa) [23]. This is mainly due to the incorporation of compressive residual stress in the film samples as commonly observed in magnetron sputtering deposited thin films.

3.4. Thermal stability of the UO_2 films

Fig. 8 shows the XRD patterns of the UO_2 thin film deposited at $f_{O_2} = 10\%$ during annealing in vacuum at 600 °C for 104 h using HSXRD. In the patterns, the Si peak came from the Si substrate. The Ti peaks came from Ti metal sponge around the film sample. The UO_2 film showed polycrystalline structure with cubic diffraction peaks. All UO_2 diffraction peaks shifted to higher diffraction angles. The peak shifting can be explained by two assumptions.

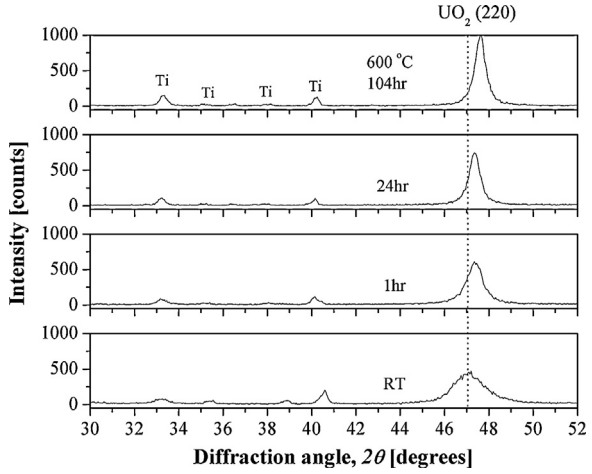

Fig. 8. In situ XRD measurements of the UO_2 film thermally annealing at 600 °C in vacuum.

One is related to the stress release in the film. The peak shifting can also be a result of the changes of the film chemical homogeneity or stoichiometry at higher temperatures. However, further accurate determination of film stoichiometry is needed for a better understanding of the changes. Additionally, the width of the peaks decreased as the annealing time was increased, indicating the grain growth in the film. However, no phase change was found for the UO_2 film after annealing at 600 °C for 104 h. This study has demonstrated the excellent thermal stability of the UO_2 thin film deposited using PDCMS.

4. Conclusions

Crystalline uranium oxide thin films with different oxide phases (UO_x ($x < 2$), UO_2, U_3O_7, and U_3O_8) were deposited by sputtering a depleted U target in an $Ar + O_2$ mixture using middle frequency pulsed dc magnetron sputtering at 500 °C. The percentage of the O_2 flow rate to the total gas flow rate (f_{O_2}) was varied from 0 to 30%, significantly varying the thin film structure. The film deposited at $f_{O_2} = 5\%$ contains a mixture of metallic U and UO_2 phases. As the f_{O_2} was controlled in a small range of 10–13%, UO_2 thin films with a (2 2 0) preferential orientation and close to stoichiometric O:U ratio of 2 were formed. A slight increase in the f_{O_2} to 15% led to the formation of metastable U_3O_7 phase in the film. Further increasing the f_{O_2} to 20% and above, the uranium oxide films exhibited a single U_3O_8 phase. The film deposited at $f_{O_2} = 10\%$ with a single UO_2 phase exhibited the maximum hardness of 14.3 GPa. No phase change was observed for the UO_2 thin film after annealing at 600 °C in vacuum for 104 h.

Acknowledgments

This work was authored by a contractor of the U.S. Government under DOE Contract No. DE-AC07-05ID14517, under the Energy Frontier Research Center (Office of Science, Office of Basic Energy Science, FWP 1356). Accordingly, the U.S. Government retains and the publisher, by accepting the article for publication, acknowledges that the U.S. Government retains a nonexclusive, paid-up, irrevocable, world-wide license to publish or reproduce the published form of this manuscript, or allow others to do so, for U.S. Government purposes. Use of the FIB and atom probe at the Center for Advanced Energy Studies was supported by the U.S. Department of Energy, Office of Nuclear Energy under DOE Idaho Operations Office Contract DE-AC07-051D14517.

References

[1] H. Idriss, Surf. Sci. Rep. 65 (2010) 67–109.
[2] C. Sari, U. Benedict, H. Blank, J. Nucl. Mater. 35 (1970) 267.
[3] S.R. Qiu, C. Amrhein, M.L. Hunt, R. Pfeffer, B. Yakshinskiy, L. Zhang, T.E. Madey, J.A. Yarmoff, Appl. Surf. Sci. 181 (2001) 211–224.
[4] P.B. Weisensee, J.P. Feser, D.G. Gahill, J. Nucl. Mater. 443 (2013) 212–217.
[5] M.M. Strehle, B.J. Heuser, M.S. Elbakhshwan, X.C. Han, D.J. Gennardo, H.K. Pappas, H. Ju, Thin Solid Films 520 (2012) 5616–5626.
[6] G.J. Hutchings, C.S. Heneghan, I.D. Hudson, S.H. Taylor, Nature 384 (1996) 341–343.
[7] T.T. Meek, B. von Roedern, P.G. Clem, R.J. Hanrahan Jr., Mater. Lett. 59 (2005) 1085–1088.
[8] I.A. Artioukov, R.M. Fechtchenko, A.L. Udovskii, Nucl. Instrum. Methods Phys. Res. Sect. A 372 (2004) 517.
[9] T.K. Bierlein, B. Mastel, J. Appl. Phys. 31 (1960) 2314–2315.
[10] H.J. Matzke, V. Nitzki, C. Ronchi, Thin Solid Films 22 (1974) 75–82.
[11] N. Popescu-Pogrion, F. Vasiliu, M.I. Birjega, J. Nucl. Mater. 51 (1974) 255–260.
[12] M.I. Bîrjega, N. Popescu-Pogrion, V. Topa, F. Vasiliu, J. Nucl. Mater. 51 (1974) 261–265.
[13] Q.X. Jia, T.M. McCleskey, A.K. Burrell, Y. Lin, G. Collis, H. Wang, A.D.Q. Li, S.R. Foltyn, Nat. Mater. 3 (2004) 529.
[14] B. Navinsek, J. Nucl. Mater. 40 (1971) 338–340.
[15] F. Miserque, T. Gouder, D.H. Wegen, P.D.W. Bottomley, J. Nucl. Mater. 298 (2001) 280–290.
[16] Q. Chen, X. Lai, B. Bai, M. Chu, Appl. Surf. Sci. 256 (2010) 3047–3050.
[17] J. Lin, J.J. Moore, B. Mishra, M. Pinks, W.D. Sproul, J.A. Rees, Surf. Coat. Technol. 202 (2008) 1418–1436.
[18] J.W. Bradley, H. Bäcker, Y. Aranda-Gonzalvo, P.J. Kelly, R.D. Arnell, Plasma Sources Sci. Technol. 11 (2002) 165.
[19] K. Thompson, D. Lawrence, D.J. Larson, J.D. Olson, T.F. Kelly, B. Gorman, Ultramicroscopy 107 (2007) 131–139.
[20] J.P. Zhao, X. Wang, Z.Y. Chen, S.Q. Yang, T.S. Shi, X.H. Liu, J. Phys. D: Appl. Phys. 30 (1997) 5–12.
[21] W.D. Sproul, D.J. Christie, D.C. Carter, Thin Solid Films 491 (2005) 1–17.
[22] J.S. Koehler, Phys. Rev. B 2 (1970) 547.
[23] K. Kurosaki, Y. Saito, H. Muta, M. Uno, S. Yamanaka, J. Alloy. Compd. 381 (2004) 240–244.